Journal of Power Sources 186 (2009) 370–376

Contents lists available at ScienceDirect

Journal of Power Sources

journal homepage: www.elsevier.com/locate/jpowsour

Performance of a proton exchange membrane fuel cell with a stepped flow field design

Chun-Hua Min*

School of Energy and Environmental Engineering, Hebei University of Technology, Tianjin 300401, PR China

ARTICLE INFO

Article history:
Received 10 October 2008
Accepted 13 October 2008
Available online 22 October 2008

Keywords:
Proton exchange membrane fuel cell
Polarization
Numerical model
Stepped flow field

ABSTRACT

A novel stepped flow field is proposed to improve the performance of a proton exchange membrane fuel cell. A three-dimensional model that accounts for activation polarization, ohmic polarization and concentration polarization is developed to achieve this. Numerical results demonstrate that overpotential values decrease in the order $\eta_{act,c} > \eta_{ohm}^{pro} > \eta_{ohm}^{el} > \eta_{act,a} > \eta_{conc,c} > \eta_{conc,a}$ at high current density. Generally, the concentration polarization can be ignored because of its low value. Using a stepped flow field improves the reactant concentration distribution, local current density distribution, water vapor concentration distribution and cell performance. If the number of steps approaches infinity, the stepped flow field extends to a tapered field that has the lowest cell performance. The lower the number of steps and the height of the outlet channel, the greater is the improvement in reactant diffusion to the porous layers, local current density distribution, water management and cell performance.

1. Introduction

The proton exchange membrane fuel cell (PEMFC) is considered a promising alternative power source to the internal combustion engine owing to its high efficiency, competitive power density, low-temperature operation, fast start-up and zero emission. A bipolar plate is a vital PEMFC component that supplies fuel and oxidant to reactive sites, removes reaction products, collects the current produced, and provides mechanical support for the cell. Bipolar plates constitute more than 60% of the weight and 30% of the total cost of a fuel cell stack [1,2].

To obtain high PEMFC performance, various flow field types have been proposed. A parallel flow field is a conventional type of flow field for which the channel is easily fabricated, but the cell performance is relatively low. Hence, some new flow field types have been investigated. Hu et al. [3] investigated the effects of the geometric parameters of a parallel flow field on a PEMFC using a mathematical model. They found that fine and close channels were beneficial for cell performance. Yoon et al. [4] also found that a narrow rib width can improve cell performance. Relative to the parallel flow field, a serpentine flow field yields better cell performance since the gas concentration is well distributed [5]. Weng et al. [6] compared the cell performance of parallel and serpentine flow fields. Their results revealed that the serpentine flow field has strong convection and high mass transfer, and hence better cell performance. However, serpentine flow fields exhibit large pressure drops and water flooding can occur quite easily [1]. Wang et al. [7] analyzed the effects of the geometric parameters of serpentine flow fields on cell performance. Their results revealed that an increase in the number of flow channel bends can improve cell performance, that a single serpentine flow field yields better performance than double and triple serpentine flow fields, and that cell performance slowly improves with increasing flow channel width. Compared to parallel and serpentine flow fields, an interdigitated flow field yields much higher cell performance since reactant transport to the diffusion and catalyst layers is mainly driven by forced convection [6,8–10]. However, interdigitated flow fields suffer from very large pressure drops. To overcome the limitations described, some new flow field types have been investigated. For instance, Kumar and Reddy [11] and Senn and Poulikakos [12] numerically simulated cell performance using a metal foam flow field and observed a more uniform local current density distribution and higher cell performance compared to parallel flow fields. Kuo et al. [13] numerically investigated PEMFC performance using a wave-like flow field and observed enhanced transport of reactant gases through the porous layer, increased gas flow velocity, and improved efficiency of the catalytic reaction. Consequently, compared to a parallel flow field, the PEMFC performance for a wave-like flow field was notably higher. Yan and co-workers [14,15] proposed a novel baffle-blocked flow field design. Baffles are arranged in the cathode flow channel to force the fuel gas to flow into the gas diffusion and catalyst layers. The results demonstrated that both reactant transport and cell performance were enhanced by the presence of baffles in the flow channel. These beneficial effects increased with increasing width

* Tel.: +86 22 60204525; fax: +86 22 60204530.
E-mail addresses: chmin@hebut.edu.cn, minchunhua@163.com.

0378-7753/$ – see front matter © 2008 Elsevier B.V. All rights reserved.
doi:10.1016/j.jpowsour.2008.10.048

Nomenclature

A	area $(m)^2$
A_s	specific area of the catalyst layer (m^{-1})
C	molar concentration mol (m^{-3})
D	diffusion coefficient $(m^2\ s^{-1})$
E	equilibrium thermodynamic potential (V)
F	Faraday constant, 96487 C (mol^{-1})
H	height (m)
i	reaction rate $(A\ m^{-3})$
I	current density $(A\ m^{-2})$
K	permeability (m^2)
L	length (m)
M	molar mass $(kg\ mol^{-1})$
n	electron number for electrochemical reactions
N	number of steps
p	pressure (Pa)
r	ratio of the outlet channel height to inlet channel height
R	resistance $(\Omega\ cm^2)$; gas constant $(8.314\ J\ mol^{-1}\ K^{-1})$
RH	relative humidity
S	source term
T	temperature (K)
$\mathbf{u}$	velocity vector $(m\ s^{-1})$
V	voltage (V)
w	velocity $(m\ s^{-1})$
W	width (m)
x, y, z	coordinate direction (m)

Greek symbols

α	transfer coefficient
β	net water transfer rate
ε	porosity
ς	stoichiometric ratio
η	overpotential (V)
κ	electrical conductivity $(S\ m^{-1})$
μ	fluid viscosity $(kg\ m^{-1}\ s^{-1})$
ρ	density of the fluid $(kg\ m^{-3})$
ω	mass fraction

Subscripts and superscripts

0	before the diffusion layer
a	anode
act	activation
av	average
c	cathode
cc	current collector
conc	concentration
ct	catalyst layer
cell	fuel cell
ch	channel
d	diffusion layer
eff	effective value
el	electron transfer
h	hydrogen
in	inlet channel
pro	ion transfer
k	species
L	limiting
m	mass and membrane
o	oxygen
ohm	ohmic polarization
out	outlet channel
ref	reference
s	specific
$\mathbf{u}$	velocity
w	water

and/or number of baffles in the tandem array. However, there is an optimum number of baffles for increasing the cell performance. Based on a fully blocked flow field, a partially blocked flow field that can obviously improve the cell performance was reported by Soong et al. [16].

The flow field designs described above can significantly improve the cell performance, but all result in a greater pressure drop compared to a parallel flow field. Recently, a novel tapered flow field was proposed by Liu et al. [17,18]. Their numerical results indicate that this tapered flow field can significantly improve the cell performance with no obvious increase in pressure drop.

Here we report on a novel stepped flow field. The height of the flow channel decreases in a stepwise manner along the main flow direction. If the number of steps is infinite, the stepped flow field extends to a tapered field. The objective of the present study was to numerically investigate PEMFC performance for this new stepped flow field design. To carry out the work, a three-dimensional, single-phase and isothermal numerical model accounting for activation polarization, ohmic polarization and concentration polarization was developed.

2. Model description

A schematic view of a PEMFC with parallel flow fields and the computational domain is shown in Fig. 1. It is assumed that the PEMFC structure is repeated periodically along the y-direction. To save computational time, a typical unit shown in the figure is taken as the computational domain. In the present study, stepped flow fields were adopted for both the anode and cathode. As an example, channels with three steps are shown in Fig. 2. In fact, the number of steps is a factor affecting PEMFC performance that is analyzed in the following sections.

The ratio of the outlet channel height to the inlet channel height, r_{ch}, is defined as follows:

$$r_{ch} = \frac{H_{out}}{H_{in}} \tag{1}$$

where H_{out} and H_{in} are the outlet and inlet channel height, respectively.

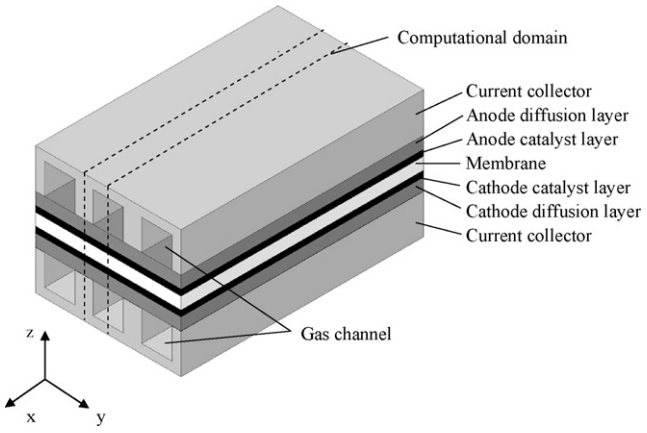

Fig. 1. Schematic view of a PEMFC.

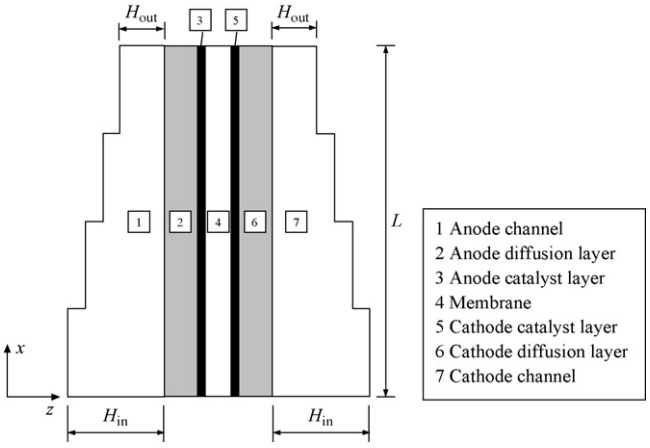

Fig. 2. A two-dimensional PEMFC in the x–z plane with a stepped flow field.

Dry air is fed into the cathode channel, whereas humidified hydrogen is supplied to the anode channel. The assumptions adopted in the present model are as follows.

(1) The fuel cell operates under steady-state and isothermal conditions;
(2) The gas mixture is an incompressible ideal fluid;
(3) The gas flow in the channels is laminar;
(4) All the porous zones in the fuel cell domain are assumed to be isotropic and homogeneous, and the membrane is considered impervious to reactant gases; and
(5) The inlet oxidant is not humidified, and water produced on the cathode side is in the gaseous state.

2.1. Governing equations

The three-dimensional model consists of non-linear, coupled partial differential equations representing the conservation of mass, momentum and species. The equations are described in vector form as follows.

The mass conservation equation can be expressed as:

$$\nabla \cdot (\rho \mathbf{u}) = S_{\mathrm{m}} \tag{2}$$

where ρ is the fluid density, $\mathbf{u}$ is the velocity vector and S_{m} is a source term for electrochemical reactions in the catalyst layers described by:

$$\text{Anode}: \quad S_{\mathrm{m,a}} = S_{\mathrm{h}} + S_{\mathrm{w,a}} \tag{3}$$

$$\text{Cathode}: \quad S_{\mathrm{m,c}} = S_{\mathrm{o}} + S_{\mathrm{w,c}} \tag{4}$$

The source terms in the above two equations will be given in the following sections.

The momentum conservation equation can be expressed as:

$$\frac{1}{\varepsilon}\nabla \cdot (\rho \mathbf{u}\mathbf{u}) = -\nabla p + \frac{1}{\varepsilon}\nabla \cdot (\mu \nabla \mathbf{u}) + S_{\mathbf{u}} \tag{5}$$

where ε is the porosity of the porous medium, p is the pressure, and $S_{\mathbf{u}}$ is the source term, which is as follows for the porous medium:

$$S_{\mathbf{u}} = -\frac{\mu}{K}\varepsilon \mathbf{u} \tag{6}$$

The species conservation equation can be expressed as:

$$\nabla \cdot (\varepsilon \rho \mathbf{u} C_k) = \nabla \cdot (\rho D_{k,\mathrm{eff}} \nabla C_k) + S_k \tag{7}$$

where the index k refers to different species, including hydrogen, oxygen and water vapor, C_k is the molar concentration of species k, and $D_{k,\mathrm{eff}}$ is the effective diffusion coefficient of species k, which can be described as follows in the porous medium [26]:

$$D_k = D_{k,\mathrm{ref}}\left(\frac{T}{T_{\mathrm{ref}}}\right)^{3/2}\left(\frac{p_{\mathrm{ref}}}{p}\right) \tag{8}$$

where $D_{k,\mathrm{eff}}$ is the reference value at T_{eff} and P_{ref}. In the porous medium region, the effective diffusivity of the species can be described by the Bruggeman model [26]:

$$D_{k,\mathrm{eff}} = \varepsilon^{1.5} \cdot D_k \tag{9}$$

S_k is the source term for electrochemical reactions in the catalyst layers, which can be expressed as:

$$S_{\mathrm{h}} = -\frac{i_{\mathrm{a}}}{2F} M_{\mathrm{h}} \tag{10}$$

$$S_{\mathrm{w,a}} = -\frac{\beta i_{\mathrm{a}}}{F} M_{\mathrm{w}} \tag{11}$$

$$S_{\mathrm{o}} = -\frac{i_{\mathrm{c}}}{4F} M_{\mathrm{o}} \tag{12}$$

$$S_{\mathrm{w,c}} = \frac{(1+2\beta) i_{\mathrm{c}}}{2F} M_{\mathrm{w}} \tag{13}$$

The cell voltage is obtained by subtracting all overpotential values from the equilibrium thermodynamic potential as follows [19]:

$$V_{\mathrm{cell}} = E - \eta_{\mathrm{act}} - \eta_{\mathrm{ohm}} - \eta_{\mathrm{conc}} \tag{14}$$

where E is the equilibrium thermodynamic potential that can be calculated using the Nernst equation [20]:

$$E = 1.23 - 0.9 \times 10^{-3}(T - 298) + 2.3\frac{RT}{4F}\log(p_{\mathrm{h}}^2 p_{\mathrm{o}}) \tag{15}$$

η_{act} is the activation overpotential, η_{ohm} is the ohmic overpotential and η_{conc} is the concentration overpotential. These parameters are discussed in detail as follows.

2.1.1. Activation overpotential

The activation overpotential comprises anode and cathode contributions. The relationship between the overpotential and the reaction rate is expressed by the Butler–Volmer equation:

$$i_{\mathrm{a}} = A_{\mathrm{s}} i_{\mathrm{a,ref}}\left(\frac{C_{\mathrm{h}}}{C_{\mathrm{h,ref}}}\right)^{1/2}\left\{\exp\left[\frac{\alpha_{\mathrm{a}} n_{\mathrm{a}} F}{RT}\eta_{\mathrm{act,a}}\right] - \exp\left[-\frac{(1-\alpha_{\mathrm{a}}) n_{\mathrm{a}} F}{RT}\eta_{\mathrm{act,a}}\right]\right\} \tag{16}$$

$$i_{\mathrm{c}} = A_{\mathrm{s}} i_{\mathrm{c,ref}}\frac{C_{\mathrm{o}}}{C_{\mathrm{o,ref}}}\left\{\exp\left[-\frac{\alpha_{\mathrm{c}} n_{\mathrm{c}} F}{RT}\eta_{\mathrm{act,c}}\right] - \exp\left[\frac{(1-\alpha_{\mathrm{c}}) n_{\mathrm{c}} F}{RT}\eta_{\mathrm{act,c}}\right]\right\} \tag{17}$$

2.1.2. Ohmic overpotential

The ohmic overpotential comprises contributions from the resistance to electron transfer and to ion transfer [21]. Based on Ohm's law, it can be expressed as:

$$\eta_{\mathrm{ohm}} = \eta_{\mathrm{ohm}}^{\mathrm{el}} + \eta_{\mathrm{ohm}}^{\mathrm{pro}} = I(R^{\mathrm{el}} + R^{\mathrm{pro}}) \tag{18}$$

where R^{el} is the resistance to electron transfer and R^{pro} is the resistance to ion transfer. R^{el} can be taken as a constant, but is generally difficult to predict [21]. Based on the computational values in Ref. [22], it is assumed that $R^{\mathrm{el}} = 0.1\ \Omega\ \mathrm{cm}^2$ in the present model.

The resistance to ion transfer can be calculated as:

$$R^{\mathrm{pro}} = \frac{H_{\mathrm{m}}}{\kappa_{\mathrm{m}}} \tag{19}$$

where H_m is the membrane height and κ_m is the membrane phase conductivity.

2.1.3. Concentration overpotential

The concentration overpotential of a PEMFC comprises anode and cathode contributions, which can be calculated as [19]:

$$\eta_{conc} = -\frac{RT}{nF}\ln\left(1-\frac{I}{I_L}\right) \quad (20)$$

where I_L is the limiting current density, and can be expressed as [23]:

$$I_L = \frac{nFD_h C_{k,0}}{H_d} \quad (21)$$

Based on the above discussions, the cell voltage can be expressed as:

$$V_{cell} = E - \eta_{act,a} - \eta_{act,c} - \eta_{ohm}^{el} - \eta_{ohm}^{pro} - \eta_{conc,a} - \eta_{conc,c} \quad (22)$$

2.2. Boundary conditions

At the gas channel inlet, the species concentrations are assumed to be constant. The inlet velocities are given by:

$$u_{a,in} = \zeta_a \frac{I_{ref}}{2F}\frac{1}{C_{h,in}}\frac{A_m}{A_{ch}} \quad (23)$$

$$u_{c,in} = \zeta_c \frac{I_{ref}}{4F}\frac{1}{C_{o,in}}\frac{A_m}{A_{ch}} \quad (24)$$

where ς_a and ς_c are the stoichiometric reactant flow ratios for the anode and cathode, respectively, and are defined as the ratio of the reactant quantity supplied to the reaction quantity generated for a specific reference current density I_{ref}. A_m is the geometrical area of the membrane and A_{ch} is the cross-sectional area of the gas channel.

A local one-way assumption is adopted to provide the channel outlet velocity condition, and is then corrected using a global mass conservation constraint [24].

At the body surface, the no-slip condition is applied for the velocity and the non-permeable condition is applied for the species mass fraction.

3. Numerical procedure

The governing equations and the boundary conditions are discretized using the finite volume method. The SIMPLEC algorithm [24] is used for coupling the velocity and pressure. Since all governing equations are coupled to one another, they should be solved simultaneously using an iterative method. The solution is considered to be convergent when the relative error for each dependent variable between two consecutive iterations is less than 1.0×10^{-5}.

The grid system is $62 \times 22 \times 56$. To simulate local transport phenomena in the fuel cell, the grid arrangement in the z-direction is non-uniform. A grid independence test was carried out for nine grid systems. Cell voltage results computed using the model under different grid systems for $I_{av} = 0.6\,A\,cm^{-2}$ are summarized in Table 1. Considering both accuracy and economics, a grid system of $62 \times 22 \times 56$ was selected for the present study.

The parameters used in the present model are listed in Table 2.

4. Results and discussion

In this section, η–I_{av} curves for a PEMFC with a parallel flow field are first presented. Then the performance of the stepped flow field for different numbers of steps is compared. Third, the effect of the outlet channel height on cell performance is discussed. Finally, the pressure drops for stepped flow fields are analyzed.

Table 1
Grid independence test ($I_{av} = 0.6\,A\,cm^{-2}$).

Stage	Grid size	V_{cell}/V
1	$52 \times 22 \times 56$	0.68360
	$62 \times 22 \times 56$	0.68361
	$72 \times 22 \times 56$	0.68362
2	$62 \times 12 \times 56$	0.68347
	$62 \times 22 \times 56$	0.68361
	$62 \times 34 \times 56$	0.68370
3	$62 \times 22 \times 40$	0.68355
	$62 \times 22 \times 56$	0.68361
	$62 \times 22 \times 64$	0.68362

4.1. Polarization curve and overpotential curves

The polarization curve and overpotential curves for a PEMFC with a parallel flow field are shown in Figs. 3 and 4, respectively. The activation polarization, ohmic polarization and concentration polarization are clearly observed in Fig. 4 and follow the general trends reported in the literature. Overpotential values decrease in the order $\eta_{act,c} > \eta_{ohm}^{pro} > \eta_{ohm}^{el} > \eta_{act,a} > \eta_{conc,c} > \eta_{conc,a}$ at high current density. The value of $\eta_{act,a}$ can be greater than that of η_{ohm}^{pro} or η_{ohm}^{el} at low current density owing to the non-linear relationship between $\eta_{act,a}$ and I_{av}. In comparison, values of the concentration overpotential are very small. For instance, when $I_{av} = 1.025\,A\,cm^{-2}$, $\eta_{conc,c} = 8.72 \times 10^{-4}$ V and $\eta_{conc,a} = 2.63 \times 10^{-3}$ V, and the sum of the

Table 2
Parameters used in the model.

Parameter	Symbol	Value	Reference
Gas channel length	L	0.06 m	
Gas channel width	W	1.0×10^{-3} m	
Gas channel height	H_{ch}	2.0×10^{-3} m	
Diffusion layer height	H_d	2.54×10^{-4} m	
Catalyst layer height	H_{ct}	2.87×10^{-5} m	
Membrane height	H_m	2.3×10^{-4} m	
Land area width	W_{cc}	1.0×10^{-3} m	
Faraday's constant	F	96,487 C mol^{-1}	
Operation temperature	T	353 K	
Anode/cathode pressure	p_a/p_c	1/1 atm	
Electron number of anode reaction	n_a	4	
Electron number of cathode reaction	n_c	2	
Fuel/air stoichiometric flow ratio	ς_a/ς_c	3/3	[25]
Relative humidity of inlet fuel	RH_a	100%	[26]
Relative humidity of inlet air	RH_c	0	[26]
Oxygen mass fraction of inlet air	ω_o	0.23	
H_2 diffusion coefficient at reference state	$D_{h,ref}$	0.915×10^{-4} m^2 s^{-1}	[25]
O_2 diffusion coefficient at reference state	$D_{o,ref}$	0.22×10^{-4} m^2 s^{-1}	[25]
Water vapor diffusion coefficient at reference state	$D_{w,ref}$	0.256×10^{-4} m^2 s^{-1}	[25]
Anode exchange current density multiply specific area	$A_s i_{a,ref}$	5.0×10^7 A m^{-3}	
Cathode exchange current density multiply specific area	$A_s i_{c,ref}$	120 A m^{-3}	
Hydrogen reference concentration	$c_{h,ref}$	56.4 mol m^{-3}	[25]
Oxygen reference concentration	$c_{o,ref}$	3.39 mol m^{-3}	[25]
Anode transfer coefficient	α_a	0.5	[26]
Cathode transfer coefficient	α_c	0.5	[26]
Porosity of diffusion layer	ε_d	0.3	[27]
Porosity of catalyst layer	ε_{ct}	0.28	[27]
Absolute permeability	K	1.76×10^{-11} m^2	[27]
Membrane phase conductivity	κ_m	17 S m^{-1}	[25]

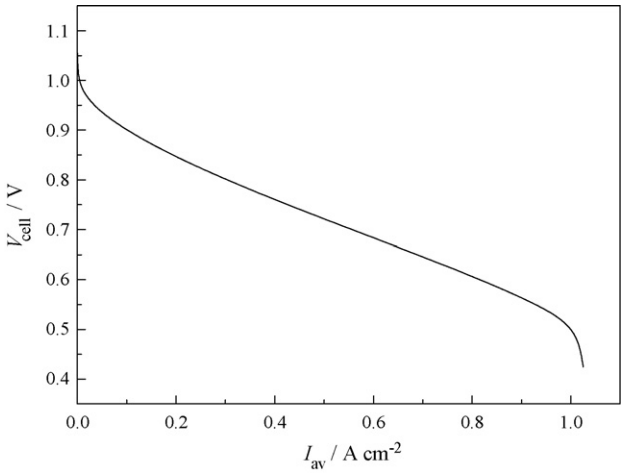

Fig. 3. Polarization curve for the PEMFC.

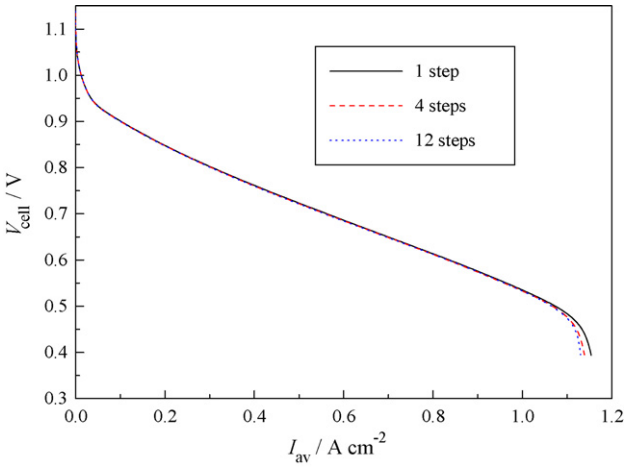

Fig. 5. Effect of N on the cell performance.

two values is approximately 4.4% of $\eta_{act,a}$. Hence the concentration overpotentials can generally be ignored.

In particular, the anode hydrogen oxidation reaction (HOR) is five orders of magnitude faster than the cathode oxygen reduction reaction (ORR), and therefore one may consider that the anode activation overpotential can be ignored. However, the electron number for the HOR is 2, which is half of the number for the ORR. In addition, the model equations are strongly non-linear. Hence, the anode activation overpotential is not negligible in terms of affecting the cell performance. Similar results have previously been reported [28].

4.2. Effect of step number on PEMFC performance

To examine the effect of the number of steps on PEMFC performance, I–V curves for $N = 1$, 4, and 12 at $r_{ch} = 1/4$ are presented in Fig. 5. It is evident that the effects of N on cell performance are negligible at low current density. However, variations in N affect cell performance to some extent at high current density. In addition, an increase in N can decrease the cell performance. Therefore, we can imagine that a stepped flow field will extend to a tapered field, as reported in Ref. [17] when N is infinite, which exhibits the lowest cell performance. Hence, a lower number of steps is beneficial for cell performance.

To explain the above results, distributions of the average oxygen concentration in the cathode catalyst layer and the cathode current density at $I_{av} = 0.8\ A\ cm^{-2}$ are shown in Figs. 6 and 7, respectively. The oxygen concentration and cathode current density gradually decrease along the flow direction for $N = 12$. When $N = 1$, the oxygen

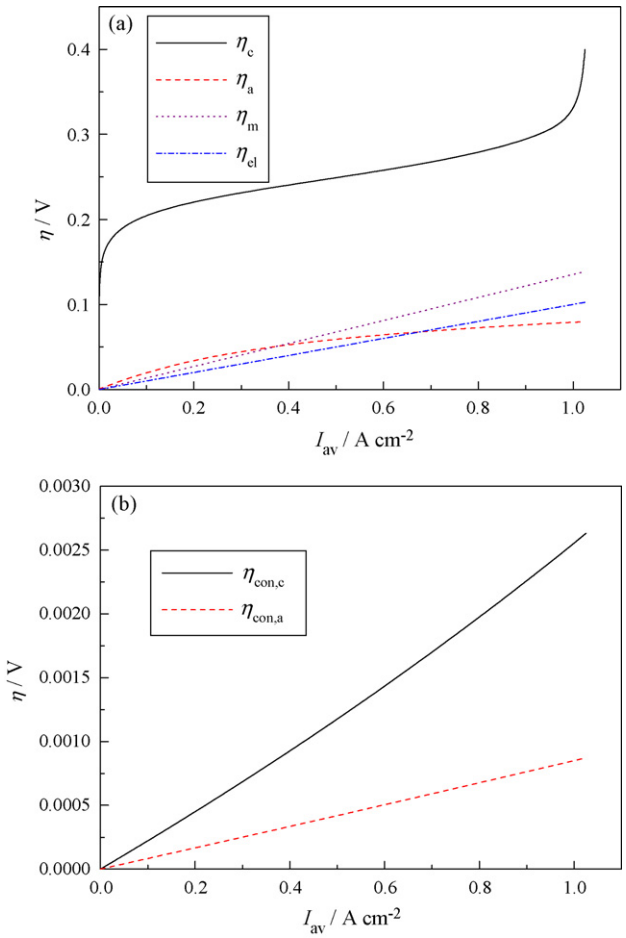

Fig. 4. Overpotential vs. average current density for (a) higher and (b) lower overpotentials.

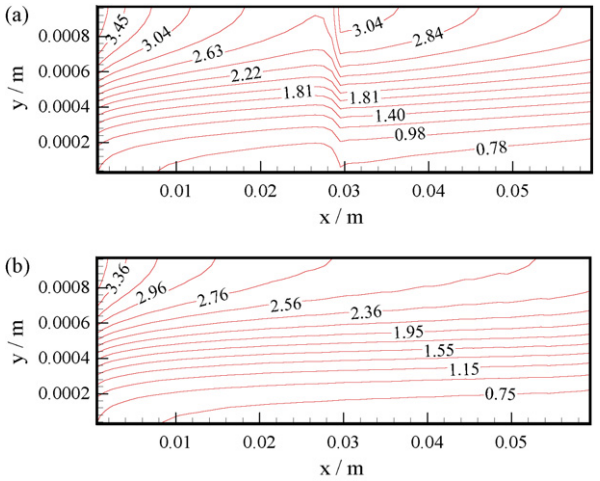

Fig. 6. Distribution of oxygen in the cathode catalyst layer ($I_{av} = 0.8\ A\ cm^{-2}$): (a) $N = 1$ and (b) $N = 12$.

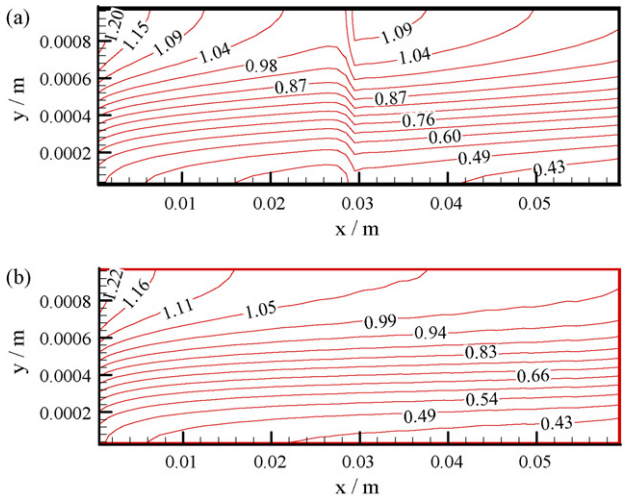

Fig. 7. Distribution of the cathode current density (I_{av} = 0.8 A cm^{-2}): (a) N = 1 and (b) N = 12.

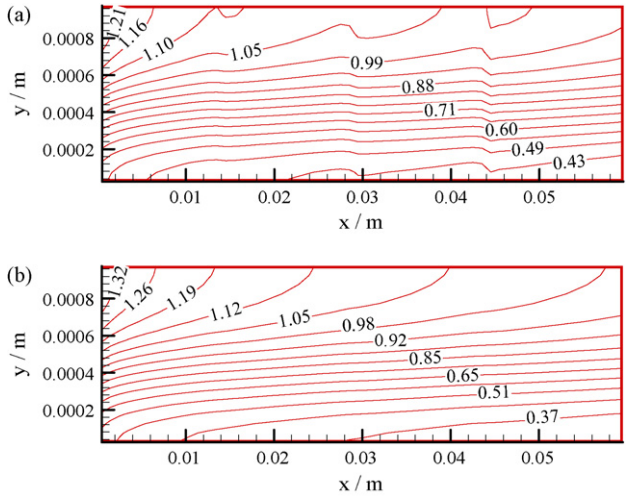

Fig. 9. Distribution of the cathode current density (N = 3, I_{av} = 0.8 A cm^{-2}): (a) r_{ch} = 4/16 and (b) r_{ch} = 13/16.

concentration and cathode current density increase significantly in the middle of the channel due to the effect of the step, i.e., the reactant gas can be forced more effectively into the porous layers for N = 1 compared to N = 12. In addition, the distributions of the oxygen concentration and cathode current density are more uniform for N = 1 than for N = 12.

4.3. Effect of outlet channel height on PEMFC performance

The effects of r_{ch} on I–V curves are shown in Fig. 8 for N = 3. It is evident that the cell performance improved with decreasing r_{ch}. As in the discussion above, the distribution of the cathode current density is used to illustrate the effects of r_{ch} on cell performance. Fig. 9 shows the distribution of the cathode current density for r_{ch} = 4/16 and 13/16. When r_{ch} is smaller, i.e., the outlet channel height is smaller, steps increase the local current density and lead to an improvement in cell performance. In addition, the smaller is r_{ch}, the more uniform is the current density distribution. The cell performance therefore improves.

Water management is very important for PEMFCs. To illustrate the high performance of the stepped flow field, the water vapor distribution at the cathode is discussed in detail. Fig. 10 shows the distribution of the average water vapor concentration in the cathode catalyst layer for r_{ch} = 4/16 and 13/16. The results demonstrate that when r_{ch} is smaller, i.e., the outlet channel height is smaller, the water vapor distribution is more uniform and the water vapor concentration is lower. These phenomena imply that a stepped flow field with small outlet channel height can effectively remove water from the fuel cell.

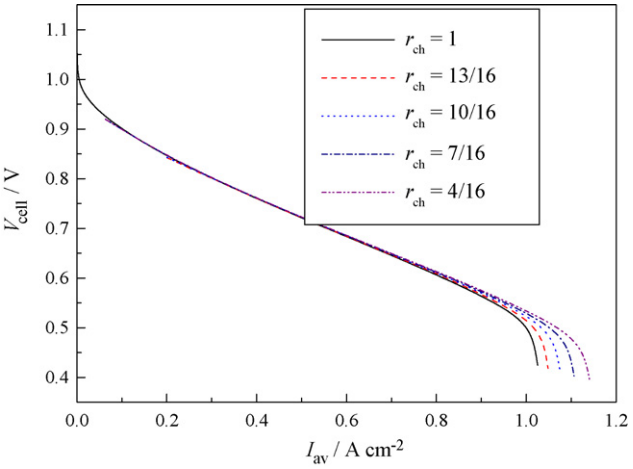

Fig. 8. Effect of r_{ch} on the cell performance (N = 3).

4.4. Pressure drop for the flow field

Finally, we consider the pressure drop for flow fields. The pressure drop between the cathode inlet channel and the outlet channel is shown in Fig. 11. As illustrated in Fig. 11(a), the pressure drop decreases significantly with the number of steps. Fig. 11(b) shows the effect of the channel height ratio, r_{ch}, on the pressure drop. A stepped flow field with a small height increases reactant diffusion into the catalyst layer and improves water removal, but increases the pressure drop. However, the maximum pressure drop is only 21 Pa in the typical cases considered in Fig. 11. This implies a small pressure drop for use of a stepped flow field.

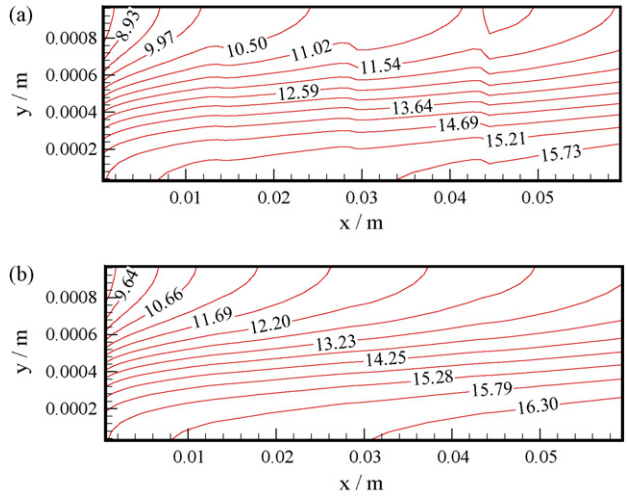

Fig. 10. Distribution of the average water vapor concentration in the cathode catalyst layer (N = 3, I_{av} = 0.8 A cm^{-2}): (a) r_{ch} = 4/16 and (b) r_{ch} = 13/16.

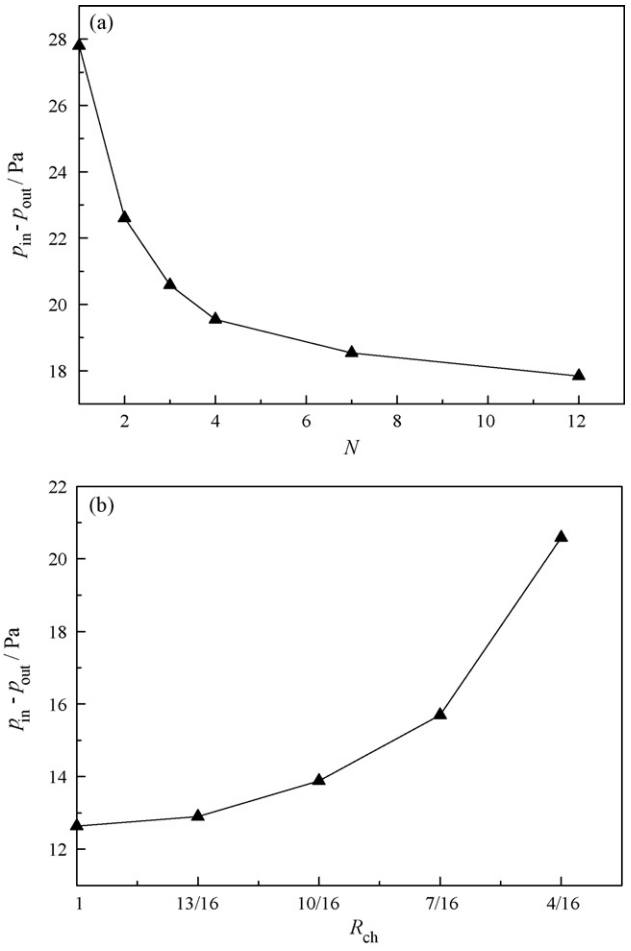

Fig. 11. Pressure drop for the stepped flow field: effect of (a) step number and (b) outlet channel height.

5. Conclusions

A new design involving a stepped flow field was proposed. The cell performance of this new design was numerically investigated. The following major conclusions can be drawn.

(1) The new model developed in this work can reasonably simulate the three overpotentials. Overpotential decreases in the order $\eta_{act,c} > \eta_{ohm}^{pro} > \eta_{ohm}^{el} > \eta_{act,a} > \eta_{conc,c} > \eta_{conc,a}$ at high current density. Generally, the concentration polarization can be ignored.

(2) The stepped flow field will extend to a tapered field if the number of steps approaches infinity. The smaller the number of steps, the more favorable is the improvement in reactant diffusion to the porous layers, local current density distribution and cell performance.

(3) A lower outlet channel height is beneficial in improving the gas flow, local current density distribution, water management and cell performance.

(4) Use of a stepped flow field can lead to a significant penalty in terms of pressure drop. However, the pressure drop observed was actually low and the cell performance was high. Hence, this new flow field can be widely adopted in the future.

Finally, it should be noted that removal of liquid water from the fuel cell is very important. More research is needed to analyze the cell performance for a two-phase and non-isothermal model.

References

[1] E. Middelman, W. Kout, B. Vogelaar, J. Lenssen, E. de Waal, J. Power Sources 118 (2003) 44–46.
[2] X. Li, I. Sabir, Int. J. Hydrogen Energy 30 (2005) 359–371.
[3] J. Hu, B. Yi, Z. Hou, Y. Cai, H. Zhang, J. Chem. Ind. Eng. (China) 55 (2004) 96–100.
[4] Y.G. Yoon, W.Y. Lee, G.G. Park, T.H. Yang, C.S. Kim, Int. J. Hydrogen Energy 30 (2005) 1363–1366.
[5] A. Su, Y.C. Chiu, F.B. Weng, Int. J. Energy Res. 29 (2005) 409–425.
[6] F.B. Weng, A. Su, G.B. Jung, Y.C. Chiu, S.H. Chan, J. Power Sources 145 (2005) 546–554.
[7] W.D. Wang, Y.Y. Duan, W.M. Yan, X.F. Peng, J. Power Sources 175 (2008) 397–407.
[8] A. Kazim, H.T. Liu, P. Forges, J. Appl. Electrochem. 29 (1999) 1409–1416.
[9] G. Hu, J. Fan, S. Chen, Y. Liu, K. Cen, J. Power Sources 136 (2004) 1–9.
[10] X.D. Wang, Y.Y. Duan, W.M. Yan, X.F. Peng, Electrochim. Acta 53 (2008) 5334–5343.
[11] A. Kumar, R.G. Reddy, J. Power Sources 114 (2003) 54–62.
[12] S.M. Senn, D. Poulikakos, J. Heat Transfer ASME 126 (2004) 410–418.
[13] J.K. Kuo, T.H. Yen, C.K. Chen, J. Power Sources 177 (2008) 96–103.
[14] H.C. Liu, W.M. Yan, C.Y. Soong, F. Chen, J. Power Sources 142 (2005) 125–133.
[15] J.H. Jang, W.M. Yan, H.Y. Li, Y.C. Chou, J. Power Sources 159 (2006) 468–477.
[16] C.Y. Soong, W.M. Yan, C.Y. Tseng, H.C. Liu, F. Chen, H.S. Chu, J. Power Sources 143 (2005) 36–47.
[17] H.C. Liu, W.M. Yan, C.Y. Soong, F. Chen, H.S. Chu, J. Power Sources 158 (2006) 78–87.
[18] W.M. Yan, H.C. Liu, C.Y. Soong, F. Chen, C.H. Cheng, J. Power Sources 161 (2006) 907–919.
[19] M.A.R. Sadiq Al-Baghdadi, H.A.K. Shahad Al-Janabi, Renew Energy 32 (2007) 1077–1101.
[20] D.M. Bernardi, M.W. Verbrugge, J. Electrochem. Soc. 139 (1992) 2477–2491.
[21] R.F. Mann, J.C. Amphlett, M.A.I. Hooper, H.M. Jensen, B.A. Peppley, P.R. Robege, J. Power Sources 86 (2000) 173–180.
[22] G. Squadrito, G. Maggio, E. Passalacqua, F. Lufrano, A. Patti, J. Appl. Electrochem. 29 (1999) 1449–1455.
[23] L.R. Jordan, A.K. Shukla, T. Behrsing, N.R. Avery, B.C. Muddle, M. Forsyth, J. Power Sources 86 (2000) 250–254.
[24] W.Q. Tao, Numerical Heat Transfer, 2nd ed., Xi'an Jiaotong University Press, Xi'an, 2001, p. 220.
[25] T. Berning, D.M. Lu, N. Djilali, J. Power Source 106 (2002) 284–294.
[26] H. Ju, H. Meng, C.Y. Wang, Int. J. Heat Mass Transfer 48 (2005) 1303–1315.
[27] X. Liu, W. Tao, Z. Li, Y. He, J. Power Sources 158 (2006) 25–35.
[28] D. Singh, D.M. Lu, N. Djilali, Int. J. Eng. Sci. 37 (1999) 431–452.